Contents lists available at ScienceDirect

# Applied Catalysis B: Environmental

# Enhancement of full-spectrum photocatalytic activity over $BiPO_4/Bi_2WO_6$ composites

Yanyan Zhu [a,b,1], Yajun Wang [c,1], Qiang Ling [b], Yongfa Zhu [a,*]

[a] Department of Chemistry, Beijing Key Laboratory for Analytical Methods and Instrumentation, Tsinghua University, Beijing 100084, PR China
[b] Institute of Aeronautical Meteorology and Chemical Defence, Beijing 100085, PR China
[c] State Key Laboratory of Heavy Oil Processing, China University of Petroleum, Beijing 102249, PR China

## ARTICLE INFO

## ABSTRACT

The full-spectrum photocatalytst is of important value for the practical use, which could absorb natural sunlight for photoctalytic degrading organic pollutants. $BiPO_4/Bi_2WO_6$ composite photocatalysts were prepared via ultrasonic-calcination method and had superior photocatalytic performance for degrading different kinds of organic pollutants under simulant sunlight irradiation. The apparent rate constant of 5.0%$BiPO_4/Bi_2WO_6$ on the degradation of methylene blue (MB) is 0.0305 $min^{-1}$, which is about 25.4 and 3.2 times of pure $BiPO_4$ and $Bi_2WO_6$ respectively. In the $BiPO_4/Bi_2WO_6$ composite photocatalysts, the core-hole structure of $BiPO_4$ as core and $Bi_2WO_6$ as hole was formed. During the photocatalytic process of $BiPO_4/Bi_2WO_6$ composites under simulant sunlight irradiation, the photo-generated electrons of $BiPO_4$ would inject to the conduction band of $Bi_2WO_6$, and the photo-generated holes on $Bi_2WO_6$ could transfer to the valance band of $BiPO_4$, and then an effective charges separation was achieved. The interaction of $BiPO_4$ and $Bi_2WO_6$ not only expanded the range of absorption spectrum but also enhanced the separation efficiency of photo-generated charges, and further improved the photocatalytic performance.

## 1. Introduction

Photocatalysis has an important value in environmental purification and energy use utilization in recent years. The study of full-spectrum photocatalyst is the key technology that makes the best use of natural sunlight to purify environment [1,2]. Recently, much attention has been given to Bi-based photocatalysts [3]. As a visible photocatalyst, $Bi_2WO_6$ possesses many advantages such as high activity, stable property and so on, which ascribes to the structure that the octahedron of ceratoid $WO_6$ locates in the sandwich of $(Bi_2O_2)^{2+}$ and promote the quick separation of photo-generated charges. $Bi_2WO_6$ has attracted more attention on the photocatalytic degradation of organic pollutants, however it still need further improve the photocatalytic efficiency in practical use [4–7]. $Bi_2WO_6$ doped with noble metal cocatalyst such as Au [8], Ag [9,10], Pt [11] or composited other semiconductor photocatalysts such as $TiO_2$ [12,13], ZnO [14], AgBr [15], $Ag_3PO_4$ [16], $BiVO_4$ [17], $Bi_2O_3$ [18] and $Co_3O_4$ [19], $C_3N_4$ [20,21] to further improve photoctalytic performance. $BiPO_4$, as a high active ultraviolent photocatalyst, has been attached importance by more and more researchers recently. Our research groups prepared three kinds of crystal structure and different morphology $BiPO_4$ photocatalysts via various methods such as hydrothermal, solvothermal, reflux and calcination, the photocatalytic activity of monazite monoclinic $BiPO_4$ is much better than that of traditional P25 $TiO_2$ [22–26]. Because the band gap of $BiPO_4$ is very wide, which only is excited by ultraviolent under 300 nm wavelength. In order to expand the absorption range and improve the photocatalytic activity, $BiPO_4$ was composited with RGO [27], $C_3N_4$ [28,29], BiOI [30,31], BiOBr [32,33], $Ag_3PO_4$ [34–36], $Bi_2MoO_6$ [37], $BiVO_4$ [38], AgBr [39], AgI [40] and so on.

Based on merits and shortcomings of $BiPO_4$ and $Bi_2WO_6$ photocatalysts, $BiPO_4/Bi_2WO_6$ composites were prepared via ultrasonic-calcination method in this work. Under the simulant sunlight irradiation, the photocatalytic activity of $BiPO_4/Bi_2WO_6$ on the degradation of different kinds of organic pollutants was evaluated. Moreover, physicochemical properties and the proposed enhancement mechanism of $BiPO_4/Bi_2WO_6$ photocatalytic activity were also systematically investigated.

## 2. Experimental section

### 2.1. Synthesis of $BiPO_4/Bi_2WO_6$ composite photocatalysts

Monazite monoclinic $BiPO_4$ nanorods prepared via reflux was used as precursor [25]. Appropriate amount $BiPO_4$ was weighed

* Corresponding author.
  E-mail address: zhuyf@mail.tsinghua.edu.cn (Y. Zhu).
[1] The first coauthors.

and added into a beaker, then 4.85 g (10 mmol) Bi(NO$_3$)$_3$·5H$_2$O and 3.3 g (10 mmol) Na$_2$WO$_6$·2H$_2$O were added as 1:1 mol ratio, at last 900 mL deionized water was added. The mixture was ultrasonicated for 1.0 h and then vigorously stirred for 1.0 h. A white precipitate was obtained by centrifugation and washed with deionized water for 3 times. Finally, the product was dried at 120 °C for 12.0 h and then calcinated in the muffle furnace in air at 500 °C for 4.0 h. According to the addition amount of BiPO$_4$, 0.5%, 1.0%, 3.0%, 5.0%, 8.0% and 10.0%BiPO$_4$/Bi$_2$WO$_6$ composite photocatalysts were obtained respectively.

## 2.2. Evaluation of photocatalytic activity and photoelectrochemical performance

The photocatalytic activity of as-prepared BiPO$_4$/Bi$_2$WO$_6$ composite photocatalysts were evaluated by degradation of MB in aqueous solution under a 500 W simulant sunlight xenon lamp irradiation (Institute for Electric Light Sources, Beijing) with no or different wavelength band-pass filter. 25 mg photocatalyst was added into as-prepared 50 mL 1.0 × 10$^{-5}$ mol L$^{-1}$ MB aqueous solution. Before irradiation, the suspension was ultrasonically dispersed for 0.5 h and then magnetically stirred for 1.0 h in dark to ensure the establishment of adsorption–desorption equilibrium. At each given time intervals, 3.0 mL suspension was taken out and separated through centrifugation (4000 rpm, 10 min). The concentration of MB solution was analyzed at the absorption band maximum (663 nm) using a Hitachi U-3010 UV vis spectrophotometer. The methods for the photocatalytic degradation of methyl orange (MO), Rhodamine B (RhB) and phenol were the same as above, but the concentration of phenol was 5.0 mg L$^{-1}$. The concentration of phenol is monitored using HPLC analysis with a UV detector at 270 nm. The mobile phase was methanol and water as 6:4, and the flow rate was 1.0 mL min$^{-1}$.

The photocurrents and electrochemical impedance spectroscopy (EIS) of BiPO$_4$/Bi$_2$WO$_6$ photocatalysts were performed on CHI–660 B electrochemical system (Shanghai, China) using a standard three-electrode cell under simulant sunlight irradiation. The ITO/samples with 20 mm × 45 mm was acted as a working electrode, a standard calomel electrode (SCE) was used as reference electrode and a platinum wire was used as the counter electrode. ITO/BiPO$_4$/Bi$_2$WO$_6$ was prepared by a dip–coating method: 6 mg BiPO$_4$/Bi$_2$WO$_6$ photocatalyst was suspended into 0.75 mL ethanol to make slurry, which was then dip–coated onto ITO glass electrode. The as–prepared electrodes were dried under ambient conditions for about 12.0 h and then calcinated at 120 °C for 5.0 h in air. Unless otherwise stated, the intensity of light at the film electrode was 1.5 mW cm$^{-2}$ and 0.1 mol L$^{-1}$ Na$_2$SO$_4$ electrolytes were used. The photoelectric responses of the sample as light-on and light-off were measured at 0.0 V. The electrochemical impedance spectroscopy (EIS) was carried out at the open circuit potential, and a sinusoidal ac perturbation of 5 mV was applied to the electrode over the frequency range of 0.05–10$^5$ Hz.

## 2.3. Materials characterization

The crystallinity and purity of BiPO$_4$/Bi$_2$WO$_6$ samples were characterized by X-ray diffraction (XRD) on a Bruker D8 Advance diffractometer (Cu Kα = 1.5418 Å, tube voltage = 40 kV, tube current = 20 mA) at a scan rate of 2° min$^{-1}$ in the 2θ range from 10° to 65°. The Ultraviolet–Visible diffuse reflectance spectroscopy (UV–vis DRS) of BiPO$_4$/Bi$_2$WO$_6$ photocatalysts were performed on Hitachi U-3010 spectrophotometer equipped with an integrated sphere attachment in the range of 200–800 nm, and BaSO$_4$ was used as reference. The particle sizes of BiPO$_4$/Bi$_2$WO$_6$ samples were measured on the HITACHI HT7700 transmission electron microscopy (TEM) with an accelerating voltage 100 kV. The EDS



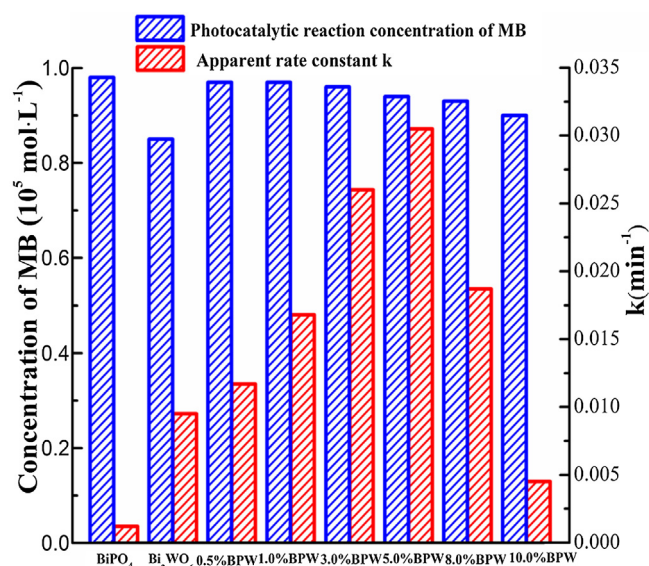**Fig. 1.** The adsorption and apparent rate constants of photocatalytic degradation MB over BiPO$_4$, Bi$_2$WO$_6$ and BiPO$_4$/Bi$_2$WO$_6$ (500 W Xenon lamp, [MB] = 1.0 × 10$^{-5}$ mol L$^{-1}$).

mapping and the lattice planes and fringes of BiPO$_4$/Bi$_2$WO$_6$ were obtained from the high-resolution transmission electron microscope (HRTEM, JEM 2010F), and it was operated at an accelerating voltage of 200 kV. The Raman spectrum was measured at room temperature using HORIBAR 800 microscopic confocal Raman spectrometer in the range of 2000 cm$^{-1}$ to 4000 cm$^{-1}$, and the excitation wavelength was the 514.5 nm from an Ar$^+$ laser with 30 mW output power. The electron spin resonance (ESR) signals of radicals spin-trapped by spin-trap reagent 5,5′-dimethyl-1-pirroline-N-oxide(DMPO) were examined on a Bruker model ESR JES-FA200 spectrometer equipped with a Quanta-Ray Nd:YAG laser system as the irradiation source (λ = 365 nm). Magnetic parameters of the radicals detected were obtained from direct measurements of magnetic field and microwave frequency.

## 3. Results and discussions

### 3.1. Photocatalytic activity and photocurrent response

BiPO$_4$ and Bi$_2$WO$_6$, as two kinds of Bi$^{3+}$ oxy-acid salt photocatalysts, have been attached great importance by more and more researchers in recent years [8,11,18,22,29]. BiPO$_4$ possesses superior ultraviolent photocatalytic performance, and Bi$_2$WO$_6$ possesses excellent visible activity. Before irradiation, the suspensions of MB over BiPO$_4$, Bi$_2$WO$_6$ and BiPO$_4$/Bi$_2$WO$_6$ composite photocatalysts were ultrasonically dispersed for 0.5 h and stirred in the dark for 1.0 h to get the adsorption-desorption equilibrium. The initial concentration of MB is 1.0 × 10$^{-5}$ mol L$^{-1}$, the initial photocatalytic reaction concentration of MB over BiPO$_4$ and Bi$_2$WO$_6$ is 0.98 × 10$^{-5}$ mol L$^{-1}$ and 0.85 × 10$^{-5}$ mol L$^{-1}$ after reaching the adsorption-desorption equilibrium (Fig. 1), which indicated that Bi$_2$WO$_6$ had more adsorption capacity of MB than BiPO$_4$. At the same time, the adsorption capacity of MB over BiPO$_4$/Bi$_2$WO$_6$ composite photocatalysts gradually decreased with the content of BiPO$_4$ increasing. The initial photocatalytic reaction concentration of MB over 5.0%BiPO$_4$/Bi$_2$WO$_6$ is 0.92 × 10$^{-5}$ mol L$^{-1}$. So the adsorption of MB over photocatasyts in this work wouldn't affect greatly the evaluation of photocatalytic performance. Under simulant sunlight irradiation, the photocatlytic activities of BiPO$_4$ and Bi$_2$WO$_6$ on the degradation of MB were very low. The apparent rate constant $k$ of BiPO$_4$ on the photocatalytic degradation of MB was
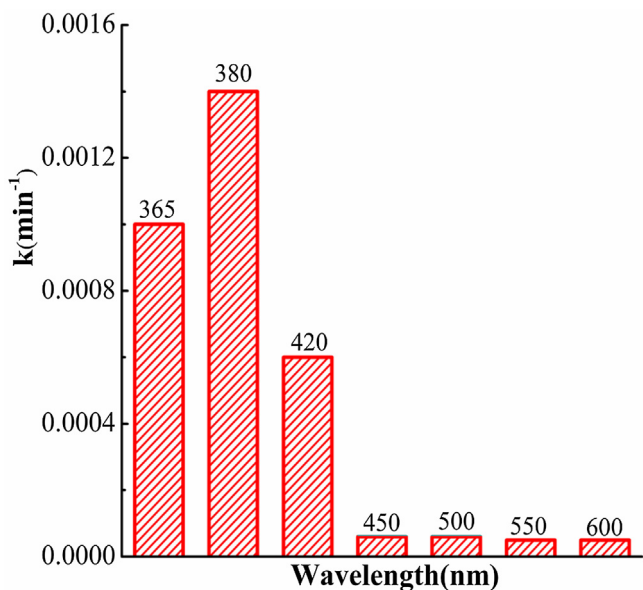
**Fig. 2.** Photocatalytic activity of 5.0%$BiPO_4$/$Bi_2WO_6$ depended on wavelength.



**Fig. 3.** Photocatalytic degradation of different kinds of organic pollutants over $Bi_2WO_6$ and 5.0%$BiPO_4$/$Bi_2WO_6$ under simulant sunlight condition (500 W Xenon lamp, 25 mg photocatalyst, [MO] = $1.0 \times 10^{-5}$ mol L$^{-1}$, [RhB] = $1.0 \times 10^{-5}$ mol L$^{-1}$, [phenol] = 5.0 ppm).

only 0.0012 min$^{-1}$, the photocatalytic activity of $Bi_2WO_6$ on the degradation of MB was higher ($k$ = 0.0095 min$^{-1}$) as a visible photocatalyst. $BiPO_4$/$Bi_2WO_6$ (BPW in Fig) composite photocatalysts possessed better photocatalytic performance on the degradation of MB under simulant sunlight irradiation. When the content of $BiPO_4$ was under 5.0%, the photocatalytic activity of $BiPO_4$/$Bi_2WO_6$ composites increased gradually with increasing the content of $BiPO_4$. The photocatalytic performance of 5.0%$BiPO_4$/$Bi_2WO_6$ was the best and its apparent rate constant $k$ was 0.0305 min$^{-1}$, which was about 25.4 and 3.2 times of pure $BiPO_4$ and $Bi_2WO_6$ respectively. When the content of $BiPO_4$ exceeded 5.0%, the photocatalytic activity of $BiPO_4$/$Bi_2WO_6$ composites decreased gradually with the content of $BiPO_4$ increasing, the above result was accorded with literatures [24,30,34,37]. Because the high content of $BiPO_4$ would reduce the absorption properties of $Bi_2WO_6$ under simulant sunlight conditions, which further decreased the photocatalytic performance of $BiPO_4$/$Bi_2WO_6$. The photocatalytic activity of 10%$BiPO_4$/$Bi_2WO_6$ was lower than that of pure $Bi_2WO_6$.

Wavelength dependent photocatalytic activities of 5.0%$BiPO_4$/$Bi_2WO_6$ were also measured in order to study its light absorption properties and the best excitation wavelength under simulant sunlight irradiation with band-pass filter. As can be seen from Fig. 2, 5.0%$BiPO_4$/$Bi_2WO_6$ had higher photocatalytic activity at 380 nm than that at 365 nm and 420 nm. Which demonstrated that 380 nm was the best excitation wavelength. With wavelength increasing above 420 nm the photocatalytic performance of 5.0%$BiPO_4$/$Bi_2WO_6$ were all very low, because long wavelength didn't excite its photo-generated charges.

$BiPO_4$/$Bi_2WO_6$ composite photocatalysts were investigated to degrade different kinds of organic pollutants popularly. $Bi_2WO_6$ and 5.0%$BiPO_4$/$Bi_2WO_6$ were selected to degrade cationic dye MO, anionic dye RhB and neutral colorless reagent phenol under simulant sunlight condition (Fig. 3). 5.0%$BiPO_4$/$Bi_2WO_6$ exhibited better photocatalytic performance on the degradation of these organic pollutants than pure $Bi_2WO_6$. The above results showed that $BiPO_4$/$Bi_2WO_6$ composite photocatalysts had no-selectivity and could effectively degrade different kinds of organic pollutants [26,41].

During the photocatalytic process, the separation and transfer of photo-generated charges are the important step that determines photocatalytic efficiency. The photocurrent responses of
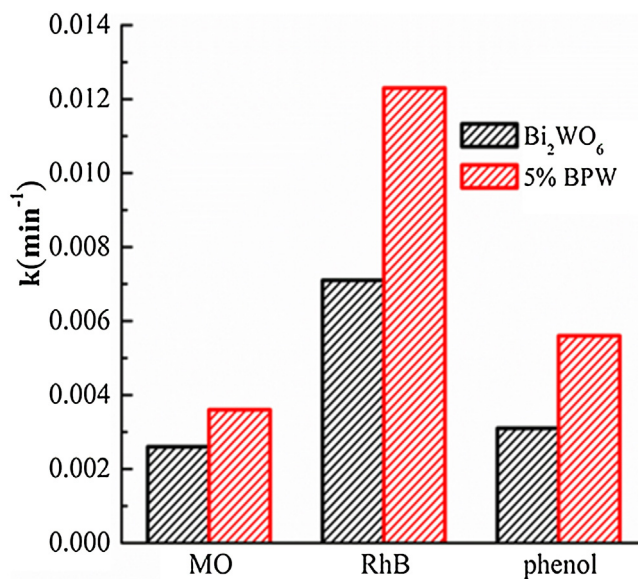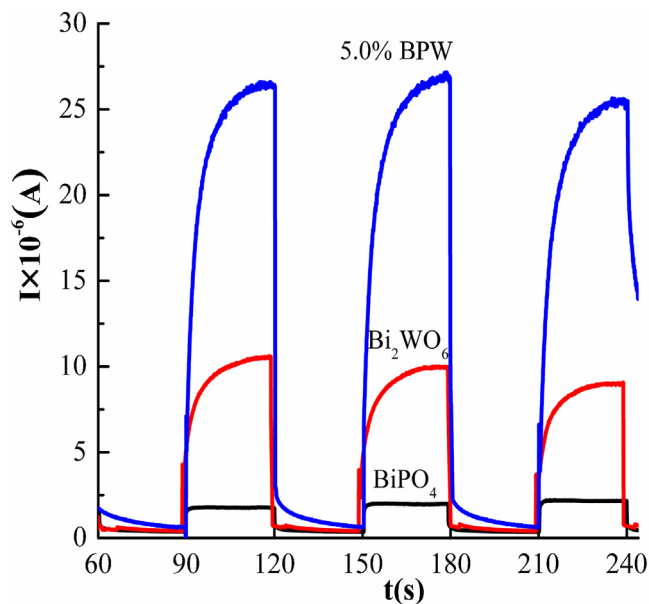


**Fig. 4.** Photocurrent responses of $BiPO_4$, 5.0%$BiPO_4$/$Bi_2WO_6$ and $Bi_2WO_6$ under simulant sunlight irradiation.

photocatalyst on the ITO conductive glass under light irradiation could demonstrate the separation and transfer efficiency of photo-generated electrons and holes [42,43]. The transient photocurrent responses of $BiPO_4$, 5.0%$BiPO_4$/$Bi_2WO_6$ and $Bi_2WO_6$ at light-on and light-off were reversible and stable (Fig. 4). Due to a little ultraviolent in the simulant sunlight, the photocurrent response of $BiPO_4$ was very weak. The photocurrent of $Bi_2WO_6$ was much better than that of $BiPO_4$. The photocurrent of 5.0%$BiPO_4$/$Bi_2WO_6$ was the highest (26 μA) and about 2.5 times as high as that of pure $Bi_2WO_6$. The enhancement of photocurrent of 5.0%$BiPO_4$/$Bi_2WO_6$ composite photocatalyst indicated that the intimate interaction was existed between $BiPO_4$ and $Bi_2WO_6$ interface, which improved the separa-
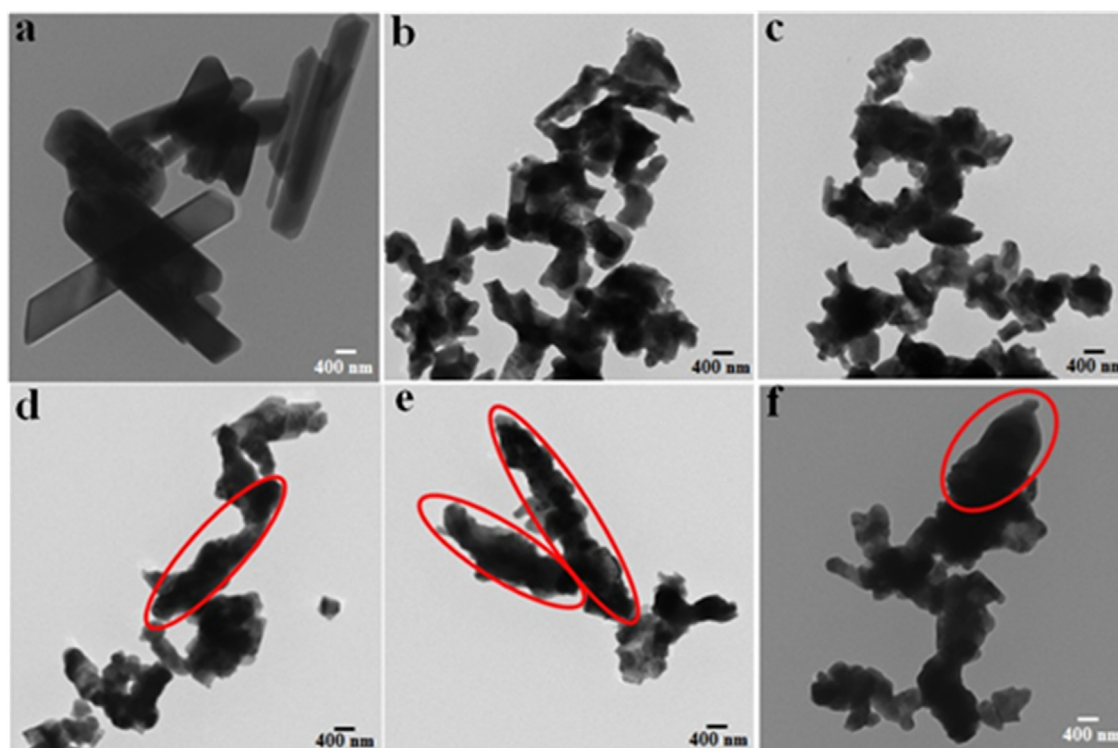
**Fig. 5.** The TEM images of $BiPO_4$, $BiPO_4/Bi_2WO_6$ composites and $Bi_2WO_6$. (a, $BiPO_4$; b, $Bi_2WO_6$; c, 1.0%$BiPO_4/Bi_2WO_6$; d 3.0%$BiPO_4/Bi_2WO_6$; e, 5.0%$BiPO_4/Bi_2WO_6$; f, 8.0%$BiPO_4/Bi_2WO_6$).
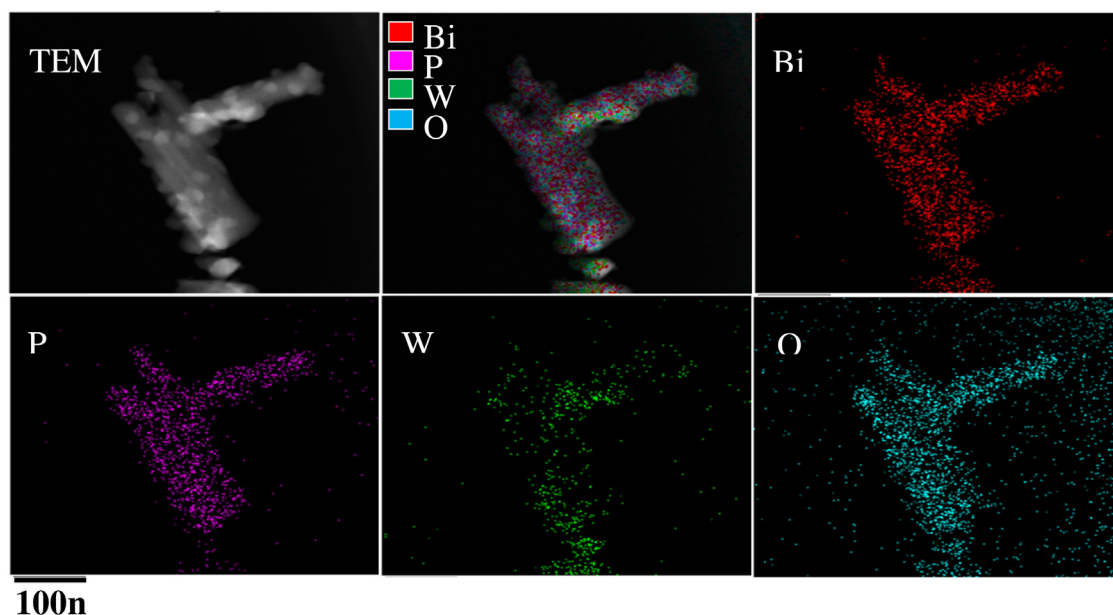


**Fig. 6.** The EDS mapping of 5.0%$BiPO_4/Bi_2WO_6$.

tion of photo-generated electrons and holes and further enhanced $BiPO_4/Bi_2WO_6$ photocatalytic performance [13,16,29,42].

### 3.2. Characterization of $BiPO_4/Bi_2WO_6$ composites

As can be seen from the TEM images that precursor $BiPO_4$ was nanorod (Fig. 5a) [25] and pure $Bi_2WO_6$ was nanosheet (Fig. 5b) [44,45]. The morphology of 1.0%$BiPO_4/Bi_2WO_6$ composite photocatalyst was the same as that of $Bi_2WO_6$ nanosheet, there was no big difference (Fig. 5c). With increasing the content of $BiPO_4$,

it can be seen that the core-hole structures of $Bi_2WO_6$ nanosheet produced around $BiPO_4$ nanorod were gradually formed from the TEM images of $BiPO_4/Bi_2WO_6$ composite photocatalysts (Fig. 5c and f). The TEM image of 5.0%$BiPO_4/Bi_2WO_6$ obviously displayed that core-hole structure of $Bi_2WO_6$ nanosheet formed around $BiPO_4$ nanorod (Fig. 5e). With the content of $BiPO_4$ further increasing, the TEM image of 8.0% $BiPO_4/Bi_2WO_6$ showed a part of bare $BiPO_4$ nanorod (Fig. 5f). It was indicated that too much content of $BiPO_4$ would destroy the core-hole structure of $BiPO_4/Bi_2WO_6$ composite

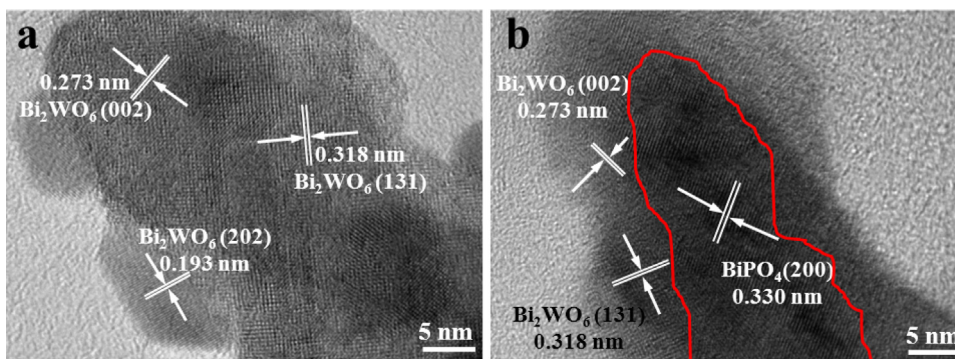**Fig. 7.** HRTEM images of $Bi_2WO_6$ (a) and $5.0\%BiPO_4/Bi_2WO_6$ (b).
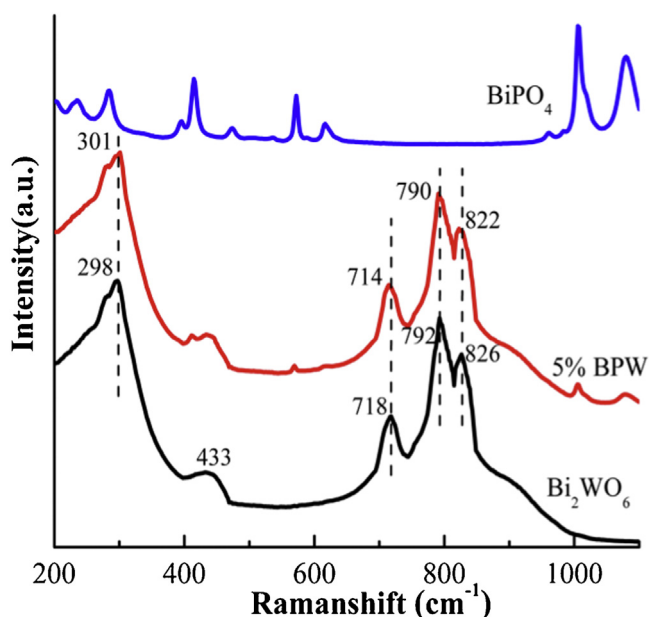


**Fig. 8.** Raman spectra of $Bi_2WO_6$, $5.0\%BiPO_4/Bi_2WO_6$ and $BiPO_4$.

photocatalysts and further decreased its absorption efficiency and photocatalytic performance.

The core-hole structure of $BiPO_4/Bi_2WO_6$ was further demonstrated by the EDS mapping and HRTEM images (Fig. 6 and Fig. 7). The elemental composition and mapping of $5.0\%BiPO_4/Bi_2WO_6$ were examined by EDS mapping (Fig. 6). Bi, P, W, O elements were all existed in $5.0\%BiPO_4/Bi_2WO_6$ composite photocatalyst. P element distributed the main body of $BiPO_4$ nanorod, but W element distributed the margin of $BiPO_4$ nanorod and a part of W elements were enriched on the surface of $BiPO_4$ nanorod. The Fig. 7a was the HRTEM image of $Bi_2WO_6$, the lattice fringes of 0.193 nm, 0.273 nm and 0.318 nm belonged to the lattice plane of $Bi_2WO_6$ orthorhombic (JPCDS 079-2381)(202),(002) and (131). From the HRTEM image of $5.0\%BiPO_4/Bi_2WO_6$, the (200) lattice plane of $BiPO_4$ about 0.330 nm lattice dispace ascribed to monazite monoclinic (JPCDS 089-0287) was coated by the (002) and (131) lattice plane of $Bi_2WO_6$. Moreover, the heterojunction was formed between the (002), (131) lattice plane of $Bi_2WO_6$ and the (200) lattice plane of $BiPO_4$.

In order to investigate the valance bond interaction between $BiPO_4$ and $Bi_2WO_6$ in $BiPO_4/Bi_2WO_6$ composite photocatalysts, the characteristic Raman spectra of samples were tested. $Bi_2WO_6$ has five characteristic Raman spectra, which located in $826\,cm^{-1}$, $792\,cm^{-1}$, $718\,cm^{-1}$, $433\,cm^{-1}$ and $298\,cm^{-1}$ respectively(Fig. 8). $826\,cm^{-1}$ and $792\,cm^{-1}$ were ascribed to the symmetric and anti-symmetric stretching modes of terminal O—W—O, the peak of

$718\,cm^{-1}$ was anti-symmetric bridging mode associated with the tungstate chain. Moreover, the peak of $433\,cm^{-1}$ was ascribed to anti-symmetric mode of $WO_6$ octahedral, the Raman peak of $298\,cm^{-1}$ was assigned to translational modes of simultaneous motions of $Bi^{3+}$ and $WO_6^{6-}$ [46–48]. The Raman spectrum of $5.0\%BiPO_4/Bi_2WO_6$ included the all characteristic peaks of $Bi_2WO_6$. Among them, the $298\,cm^{-1}$ peak of $Bi_2WO_6$ produced a red shift to $301\,cm^{-1}$, but the peaks located at $826\,cm^{-1}$, $792\,cm^{-1}$, $718\,cm^{-1}$ produced a little blue shift. It was indicated that $BiPO_4$ changed the chemical bond energy of $Bi_2WO_6$ in the $BiPO_4/Bi_2WO_6$ composite photocatalysts. There was chemical bond interaction between $BiPO_4$ and $Bi_2WO_6$. Moreover, the characteristic Raman peaks of $BiPO_4$ located at $414\,cm^{-1}$, $572\,cm^{-1}$, $1006\,cm^{-1}$ and $1079\,cm^{-1}$ appeared in the Raman peaks of $5.0\%BiPO_4/Bi_2WO_6$ [26]. The composite of $BiPO_4/Bi_2WO_6$ didn't change the crystal structure of $BiPO_4$ and $Bi_2WO_6$, and the all characteristic peaks of $Bi_2WO_6$ orthorhombic (JPCDS 079-2381) appeared. With increasing the content of $BiPO_4$, the characteristic peaks of its monazite monoclinic (JPCDS 089-0287)were gradually demonstrated (Fig. S1).

The UV–vis spectra of $BiPO_4$, $Bi_2WO_6$ and $5.0\%BiPO_4/Bi_2WO_6$ were shown in Fig. 9. The absorption band edge of precursor $BiPO_4$ was about 320 nm (Fig. 9a) [25]. $Bi_2WO_6$, as a visible photocatalyst, its absorption band edge was about 460 nm. In the range of 200–450 nm, the strong absorption of $Bi_2WO_6$ ascribed to the charge transfer from $O^{2-}$ to $W^{6+}$ [4,10]. The absorption band edge of $5.0\%BiPO_4/Bi_2WO_6$ composite photocatalyst was about 385 nm, which induced an obvious red shift compared to $BiPO_4$ and a blue shift compared to $Bi_2WO_6$. The above results illustrated that there was chemical interaction between $Bi_2WO_6$ and $BiPO_4$ interface, which improved the separation and transfer of photo-generated charges. According to the calculated Tauc's plot, the band gaps of $Bi_2WO_6$, $5.0\%BiPO_4/Bi_2WO_6$ and $BiPO_4$ were 2.7 eV, 3.2 eV and 3.9 eV respectively (Fig. 9b).

### 3.3. Proposed enhancement mechanism of $BiPO_4/Bi_2WO_6$ photocatalytic activity

The separation of photo-generated electrons and holes played a very important role during the photocatalytic process of decomposition of organic pollutants, which could be evaluated by the typical electrochemical impedance spectra (EIS) [21,26,29,41]. Under simulant sunlight irradiation and in dark, The EIS Nyquist plots of $BiPO_4$, $Bi_2WO_6$ and $5.0\%BiPO_4/Bi_2WO_6$ were presented in Fig. 10. The arc radius on the EIS spectra reflects the solid state interface layered resistance and the surface charges transfer resistance. The smaller arc radius on the EIS Nyquist plot indicates a more efficient separation of the photo-generated electrons and holes, and vice versa. The Nyquist arc radii of $5.0\%BiPO_4/Bi_2WO_6$ were all smaller than that of $BiPO_4$ and $Bi_2WO_6$, which illustrated that $BiPO_4/Bi_2WO_6$ composite photocatalyst had smaller electric
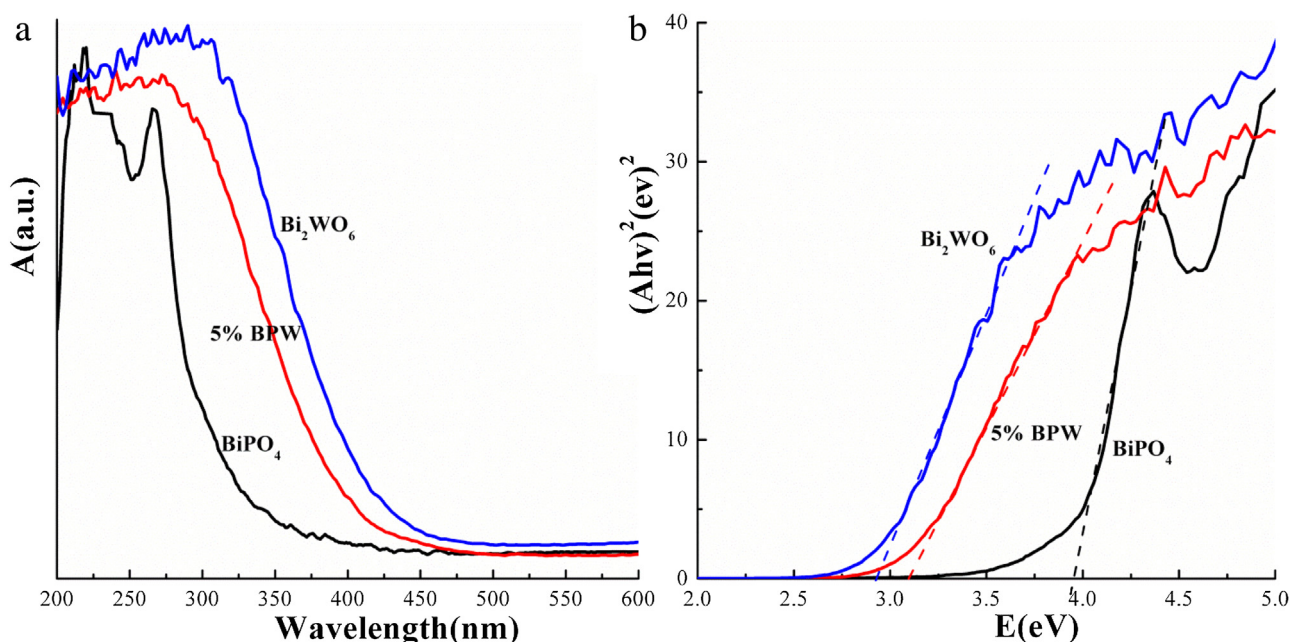
**Fig. 9.** UV–vis spectra of $Bi_2WO_6$, $5.0\%BiPO_4/Bi_2WO_6$ and $BiPO_4$.



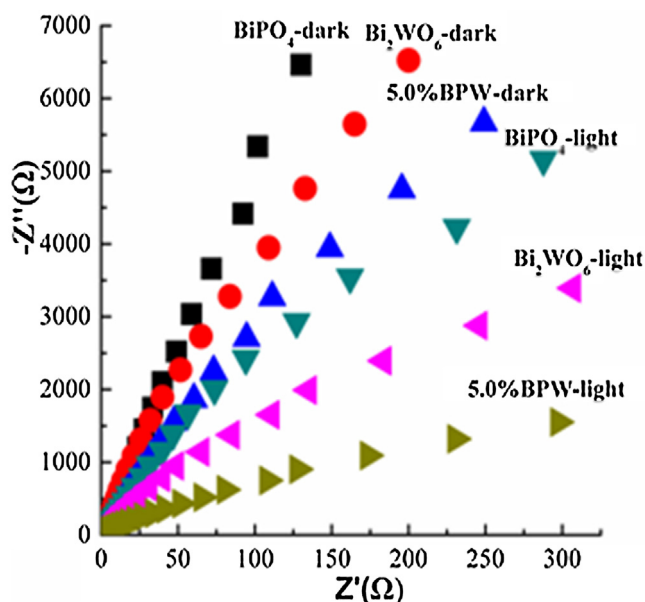**Fig. 10.** The EIS response of $Bi_2WO_6$, $5.0\%BiPO_4/Bi_2WO_6$ and $BiPO_4$ thin film electrodes in dark and under simulant sunlight irradiation.

resistance and higher efficiency of charges separation than $BiPO_4$ and $Bi_2WO_6$. Thus, $5.0\%BiPO_4/Bi_2WO_6$ photocatalyst has higher separation efficiency of photo-generated charges and better photocatalytic activity.

The main oxidative species of semiconductor photocatalysts could be verified by the trapping experiments of active species, usually using ethylenediamine tetraacetic acid disodium salt (EDTA-2Na) as hole scavengers, tertiary butyl alcohol (t-BuOH) as hydroxyl radical scavengers and purging $N_2$ as $\bullet O^{2-}$ radical scavenger. The oxidative species on the photocatalytic degradation of MB over $Bi_2WO_6$ and $5.0\%BiPO_4/Bi_2WO_6$ were shown in Fig. 11. When the $N_2$ was purged the photocatalytic activity of $Bi_2WO_6$ and $5.0\% BiPO_4/Bi_2WO_6$ didn't change, which indicated that $\bullet O^{2-}$ radical wasn't the main oxidative species. The photocatalytic per-

formance of $Bi_2WO_6$ and $5.0\%BiPO_4/Bi_2WO_6$ changed slightly by addition of t-BuOH, suggesting that $\bullet OH$ radical played an assistant role on the photocatalytic degradation of MB over $Bi_2WO_6$ and $5.0\%BiPO_4/Bi_2WO_6$. Moreover, the ESR spin-trap technique was used to monitor the oxidative species generated by $Bi_2WO_6$ and $5.0\%BiPO_4/Bi_2WO_6$ with DMPO in water and Methyl alcohol under light irradiation (Fig. S2). The result of ESR further demonstrated that there was no $\bullet O^{2-}$ radical in the system of $Bi_2WO_6$ and $5.0\%BiPO_4/Bi_2WO_6$. However, the intensity of $\bullet OH$ radical in $5.0\%BiPO_4/Bi_2WO_6$ system was much higher than that of $Bi_2WO_6$. The photocatalytic activity of $Bi_2WO_6$ and $5.0\%BiPO_4/Bi_2WO_6$ decreased greatly by addition of EDTA-2Na, which improved that photo-generated holes are the main oxidative species of $Bi_2WO_6$ and $5.0\%BiPO_4/Bi_2WO_6$.

Based on the above results, a proposed enhancement mechanism of charges separation and photocatalytic process over $BiPO_4/Bi_2WO_6$ was inferred in Fig. 12. During the photocatalytic process of $BiPO_4/Bi_2WO_6$ composites under simulant sunlight irradiation, $Bi_2WO_6$ could absorb visible light to form photo-generated holes that transited to the valance band of $BiPO_4$, at the same time $BiPO_4$ could absorb ultraviolet to form photo-generated electrons that transited to the conduction band of $Bi_2WO_6$. The interaction of $BiPO_4$ and $Bi_2WO_6$ not only expanded the range of absorption spectrum but also enhanced the separation and transfer efficiency of photo-generated charges, and then further improving the photocatalytic performance. According to the result of main oxidative species detection, the photo-generated holes of $BiPO_4$ valance band could degrade the organic pollutants directly or react with water to form $\bullet OH$ radical that further decompose organic pollutants.

## 4. Conclusions

In this work, $BiPO_4/Bi_2WO_6$ composite photocatalysts were prepared via ultrasonic-calcination method. Compared with pure $BiPO_4$ and $Bi_2WO_6$, $BiPO_4/Bi_2WO_6$ has superior photocatalytic performance for degrading different kinds of organic pollutants under simulant sunlight irradiation. In the $BiPO_4/Bi_2WO_6$ composite photocatalysts, the core-hole structure of $BiPO_4$ as core and $Bi_2WO_6$ as hole was formed. The photo-generated electrons of $BiPO_4$ would
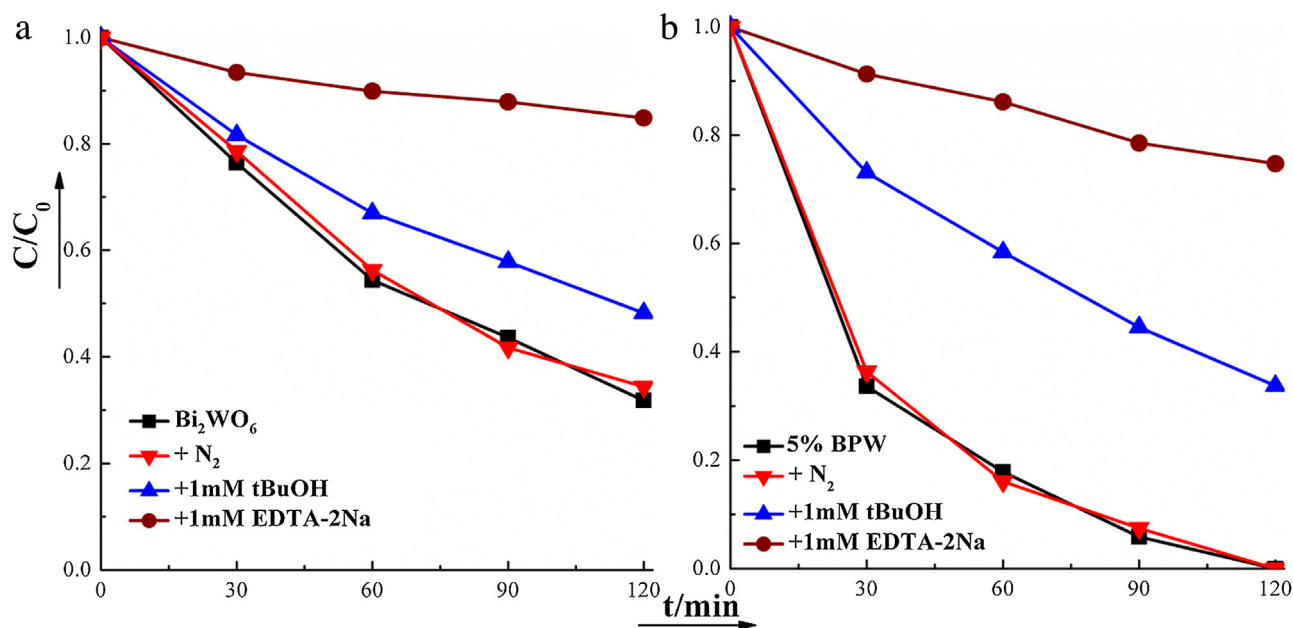
**Fig. 11.** The plots of photocatalytic degradation of MB over $Bi_2WO_6$(a)and 5.0%$BiPO_4$/$Bi_2WO_6$ (b) with the addition of hole, $\cdot O^{2-}$ and $\cdot OH$ radical scavenger under simulant sunlight irradiation.



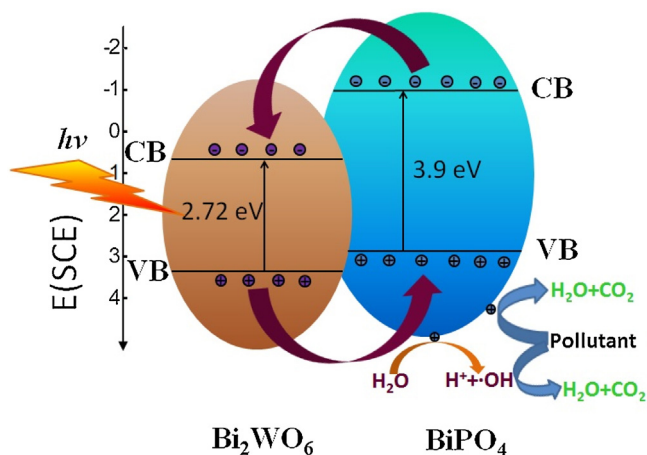**Fig. 12.** The proposed mechanism of charges separation and enhancement of $BiPO_4$/$Bi_2WO_6$ photocatalytic activity.

inject to conduction band of $Bi_2WO_6$, and the photo-generated holes on $Bi_2WO_6$ could transfer to the valance band of $BiPO_4$, and then an effective charges separation was achieved. The interaction of $BiPO_4$ and $Bi_2WO_6$ not only expanded the range of absorption spectrum but also enhance the separation efficiency of photo-generated charges, which then improve the photocatalytic performance.

### Acknowledgements

### Appendix A. Supplementary data

Supplementary data associated with this article can be found, in the online version, at http://dx.doi.org/10.1016/j.apcatb.2016.07.002.

### References

[1] A. Tang, Y. Jia, S. Zhang, Q. Yu, X. Zhang, Catal. Commun. 50 (2014) 1–4.
[2] D. Spasiano, R. Marotta, Appl. Catal. B: Environ. 170–171 (2015) 90–123.
[3] R.a. He, S. Cao, P. Zhou, J. Yu, Chin. J. Catal. 35 (2014) 989–1007.
[4] Y. Liu, H. Lv, J. Hu, Z. Li, Mater. Lett. 139 (2015) 401–404.
[5] S. Hu, C. Xu, W. Wang, F. Ma, L. Zhen, Ceram. Int. 40 (2014) 11689–11698.
[6] K. Akihiko, s. Hijii, Chem. Lett. 28 (1999) 1103–1104.
[7] X. Chu, G. Shan, C. Chang, Y. Fu, L. Yue, L. Zhu, Front. Environ. Sci. Eng. 10 (2016) 211–218.
[8] J. Liu, Y. Bai, P. Wang, Micro Nano Lett. 8 (2013) 90–93.
[9] J. Lin, Z. Guo, Z. Zhu, Ceram. Int. 40 (2014) 6495–6501.
[10] Z. Zhang, W. Wang, E. Gao, S. Sun, L. Zhang, J. Phys. Chem. C 116 (2012) 25898–25903.
[11] R.M. Mohameda, E.S. Aazam, Mater. Res. Bull. 48 (2013) 3572–3578.
[12] J. Zhang, Z. Huang, Y. Xu, F. Kang, Int. J. Photoenergy (2012).
[13] M. Shang, W. Wang, L. Zhang, S. Sun, L. Wang, L. Zhou, J. Phys. Chem. C 113 (2009) 14727–14731.
[14] X. Liu, Q. Lu, J. Liu, J. Alloys Compd. 662 (2016) 598–606.
[15] D. Wang, L. Guo, Y. Zhen, L. Yue, G. Xue, F. Fu, J. Mater. Chem. A 2 (2014) 11716–11727.
[16] G. Fu, G. Xu, S. Chen, L. Lei, M. Zhang, Catal. Commun. 40 (2013) 120–124.
[17] S. Xue, Z. Wei, X. Hou, W. Xie, S. Li, X. Shang, D. He, Appl. Surf. Sci. 355 (2015) 1107–1115.
[18] M. Gui, W. Zhang, Q. Su, C. Chen, J. Solid State Chem. 184 (2011) 1977–1982.
[19] Q. Xiao, J. Zhang, C. Xiao, X. Tan, Catal. Commun. 9 (2008) 1247–1253.
[20] M. Li, L. Zhang, X. Fan, Y. Zhou, M. Wu, J. Shi, J. Mater. Chem. A 3 (2015) 5189–5196.
[21] Y. Wang, X. Bai, C. Pan, J. He, Y. Zhu, J. Mater. Chem. 22 (23) (2012) 11568–11573.
[22] C. Pan, D. Li, X. Ma, Y. Chen, Y. Zhu, Catal. Sci. Technol. 1 (2011) 1399–1405.
[23] C. Pan, Y. Zhu, Environ. Sci. Technol. 44 (2010) 5570–5574.
[24] C. Pan, Y. Zhu, Catal. Sci. Technol. 5 (2015) 3071–3083.
[25] Y. Zhu, Y. Liu, Q. Ling, Y. Lv, H. Wang, Y. Zhu, Acta Phys. –Chim. Sin. 29 (2013) 576–584.
[26] Y. Zhu, Y. Liu, Y. Lv, Q. Ling, D. Liu, Y. Zhu, J. Mater. Chem. A 2 (2014) 13041–13048.
[27] J. Qian, Z. Yang, C. Wang, K. Wang, Q. Liu, D. Jiang, Y. Yan, K. Wang, J. Mater. Chem. A 3 (2015).
[28] Z. Li, S. Yang, J. Zhou, D. Li, X. Zhou, C. Ge, Y. Fang, Chem. Eng. J. 241 (2014) 344–351.
[29] C. Pan, J. Xu, Y. Wang, D. Li, Y. Zhu, Adv. Funct. Mater. 22 (2012) 1518–1524.
[30] Y. Liu, W. Yao, D. Liu, R. Zong, M. Zhang, X. Ma, Y. Zhu, Appl. Catal. B: Environ. 163 (2015) 547–553.
[31] J. Cao, B. Xu, H. Lin, S. Chen, Chem. Eng. J. 228 (2013) 482–488.
[32] W. An, W. Cui, Y. Liang, J. Hu, L. Liu, Appl. Surf. Sci. 351 (2015) 1131–1139.
[33] F. Duo, C. Fan, Y. Wang, Y. Cao, X. Zhang, Mater. Sci. Semicond. Process. 38 (2015) 157–164.
[34] S. Wu, H. Zhengn, Y. Wu, W. Lin, T. Xu, M. Guan, Ceram. Int. 40 (2014) 14613–14620.

[35] N. Mohaghegh, E. Rahimi, M.R. Gholami, Mater. Sci. Semicond. Process. 39 (2015) 506–514.

[36] N. Mohaghegh, M. Tasviri, E. Rahimi, M.R. Gholami, Appl. Surf. Sci. 351 (2015) 216–224.

[37] X. Lin, D. Liu, X. Guo, N. Sun, S. Zhao, L. Chang, H. Zhai, Q. Wang, J. Phys. Chem. Solids 76 (2015) 170–177.

[38] S. Ganguli, C. Hazra, M. Chatti, T. Samanta, Langmuir 32 (2016) 247–253.

[39] H. Xu, Y. Xu, H. Li, J. Xia, J. Xiong, S. Yin, C. Huang, H. Wan, Dalton Trans. 41 (2012) 3387–3394.

[40] H. Ye, H. Lin, J. Cao, S. Chen, Y. Chen, J. Mol. Catal. A: Chem. 397 (2015) 85–92.

[41] Y. Lv, Y. Zhu, Y. Zhu, J. Phys. Chem. C 117 (2013) 18520–18528.

[42] H. Huang, L. Liu, Y. Zhang, N. Tian, J. Alloys Compd. 619 (2015) 807–811.

[43] Z. Pei, S. Weng, P. Liu, Appl. Catal. B: Environ. 180 (2016) 463–470.

[44] L. Zhou, W. Wang, L. Zhang, J. Mol. Catal. A: Chem. 268 (2007) 195–200.

[45] F. Zhang, F. Xie, J. Liu, W. Zhao, K. Zhang, Ultrason. Sonochem. 20 (2013) 209–215.

[46] M. Ge, L. Liu, Mater. Sci. Semicond. Process. 25 (2014) 258–263.

[47] A. Phuruangrat, P. Dumrongrojthanath, N. Ekthammathat, S. Thongtem, T. Thongtem, J. Nanomater. 36 (2014) 1–7.

[48] R. Shi, G. Huang, J. Lin, Y. Zhu, J. Phys. Chem. C 113 (2009) 19633–19638.